HHS Public Access

Author manuscript

Sci Signal. Author manuscript; available in PMC 2017 August 15.

Published in final edited form as:

Sci Signal. ; 10(477): . doi:10.1126/scisignal.aai8133.

Hyperactive locomotion in a *Drosophila* model is a functional readout for the synaptic abnormalities underlying fragile X syndrome

Risa Kashima[1,*], **Patrick L. Redmond**[1,*], **Prajakta Ghatpande**[1], **Sougata Roy**[2], **Thomas B. Kornberg**[1], **Thomas Hanke**[3], **Stefan Knapp**[3,4], **Giorgio Lagna**[1], and **Akiko Hata**[1,†]

[1]Cardiovascular Research Institute, University of California, San Francisco, San Francisco, CA 94158, USA

[2]Department of Cell Biology and Molecular Genetics, University of Maryland, College Park, MD 20742, USA

[3]Institute of Pharmaceutical Chemistry and Buchmann Institute for Life Sciences, Goethe University, Frankfurt, Germany

[4]Department of Clinical Medicine, Structural Genomics Consortium, University of Oxford, Oxford OX3 7DQ, U.K

Abstract

Fragile X syndrome (FXS) is the most common cause of heritable intellectual disability and autism and affects ~1 in 4000 males and 1 in 8000 females. The discovery of effective treatments for FXS has been hampered by the lack of effective animal models and phenotypic readouts for drug screening. FXS ensues from the epigenetic silencing or loss-of-function mutation of the *fragile X mental retardation 1* (*FMR1*) gene, which encodes an RNA binding protein that associates with and represses the translation of target mRNAs. We previously found that the activation of LIM kinase 1 (LIMK1) downstream of augmented synthesis of bone morphogenetic protein (BMP) type 2 receptor (BMPR2) promotes aberrant synaptic development in mouse and *Drosophila* models of FXS and that these molecular and cellular markers were correlated in patients with FXS. We report that larval locomotion is augmented in a *Drosophila* FXS model. Genetic or pharmacological intervention on the BMPR2-LIMK pathway ameliorated the synaptic abnormality and locomotion phenotypes of FXS larvae, as well as hyperactivity in an FXS mouse model. Our study demonstrates that (i) the BMPR2-LIMK pathway is a promising therapeutic target for FXS and (ii) the locomotion phenotype of FXS larvae is a quantitative functional readout for the neuromorphological phenotype associated with FXS and is amenable to the screening novel FXS therapeutics.

†Corresponding author. akiko.hata@ucsf.edu.
*These authors contributed equally to this work.

Author contributions: R.K., P.L.R., S.R., P.G., T.H., S.K., T.B.K., and G. L. designed and performed the experiments and interpreted the data. R.K., P.L.R., T.B.K., S.R., T.H., S.K., and G.L. edited the manuscript. A.H. conceived the project, designed the experiments, interpreted the data, and wrote the manuscript. Competing interests: The authors declare that they have no competing interests.

SUPPLEMENTARY MATERIALS
www.sciencesignaling.org/cgi/content/full/10/477/eaai8133/DC1

INTRODUCTION

Fragile X syndrome (FXS) is linked to other neurologic and psychiatric disorders and is the most prevalent monogenetic cause of autism (1, 2). It is caused by an expansion of a triplet (CGG) more than 200 repeats in the 5′ untranslated region of *fragile X mental retardation 1* (*FMR1*), which silences its expression (1, 3). The fragile X mental retardation protein (FMRP) binds various mRNA targets and itself inhibits mRNA stability and function, including translation (3). FXS patients exhibit abnormal dendritic spine density and morphology in the central nervous system (CNS), which leads to cognitive impairment, anxiety, hyperactivity, and autistic behavior (1–3). It has been proposed that, during brain development, FMRP plays a role in dendritic spine development by repressing the translation of molecules critical for cytoskeleton remodeling and receptor signaling.

The search for an animal model of FXS has led to the generation and characterization of *Drosophila* and rodent *FMR1* mutants. It has been reported that *Drosophila* third-instar larvae with a mutation of the *Drosophila* ortholog of *FMR1* (*dFMR1*) have an increased number of branches and synaptic boutons at neuromuscular junctions (NMJs) (4). We found that the branching and bouton abnormalities were reduced by decreasing the gene dosage of the *Drosophila* ortholog of *bone morphogenetic protein receptor type 2* (*BMPR2*) gene, *wishful thinking* (*Wit*), suggesting that excess production of BMPR2 and of its downstream signaling plays a role in aberrant synaptic growth (5).

Homozygous deletion of *FMR1* (*FMR1-KO*) in rodents produces a dendritic spine abnormality that resembles the phenotype seen in FXS patients (6, 7). Furthermore, *FMR1-KO* mice and rats exhibit cognitive and behavioral traits, some of which are consistent with those of the FXS patients, such as hyperactivity as well as learning and memory defects (8). Hyperactivity is one of the hallmark characteristics of human FXS. *FMR1-KO* mice also show abnormal locomotor activity and behavioral hyperactivity (8). Therefore, locomotor hyperactivity has been used as a measurement to assess drug effect on FXS in preclinical studies. An open-field test (OFT) is one of the most commonly used mouse behavioral tests to observe locomotor activity and hyperactivity as well as anxiety. Unfortunately, the behavioral and cognitive traits of the rodent models of FXS are highly variable depending on age, gender, and strain of the animals (8). These are major limitations for the development of therapies for FXS. In addition, the behavioral tests using rodents require cost and time. Thus, there continues to be a pressing need for rapid, quantitative, sensitive, and time- and cost-effective animal assays to screen drugs for treatment of FXS, possibly using an invertebrate FXS model.

Our work that implicates BMPR2 in FXS suggests that BMPR2 may be a novel target for controlling FMRP-dependent translational regulation in FXS development (5). Both the *FMR1*-KO mouse and human FXS patients exhibit an increased abundance of BMPR2 protein in CNS neurons (5). In addition, increased BMPR2 results in activation of LIM kinase 1 (LIMK1), which interacts with the cytoplasmic domain of BMPR2 and promotes actin remodeling and dendritic spine abnormalities (5). Reduction of the *BMPR2* gene dosage as well as pharmacological inhibition of LIMK1 ameliorate the aberrant spine

development in the *FMR1-KO* mouse (5), but there have been no reported characterizations of LIMK1 inhibition on cognitive and behavioral traits of FXS model animals.

Behavioral manifestations in the *Drosophila* FXS model have been reported (9, 10) and include abnormal crawling and locomotion of third-instar larvae. Here, we developed quantitative behavioral assays that showed that reduction of *Wit* gene dosage in *dFMR1* mutant larvae reverts the locomotion phenotype and that oral administration of LIMK antagonists and a protein synthesis inhibitor restores normal crawling velocity and reduces NMJ bouton numbers. We also confirmed that administration of a LIMK antagonist in the mouse FXS model rescues the rodent behavioral abnormalities. Thus, this study demonstrates that (i) the locomotion phenotype in *dFMR1* mutant larvae serves as a readout of NMJ bouton phenotype; (ii) the larval crawling assay system that we developed can be used for the genetic or chemical screening of therapeutic molecules for FXS as well as other synapse formation abnormalities; and (iii) targeting the LIMK1 pathway, which is conserved from *Drosophila* to human, is a potential therapeutic strategy for FXS.

RESULTS

Correlation between larval locomotion activity and synaptic bouton number

A loss-of-expression mutation of *dFMR1* (*dFMR1*$^{\Delta 113}$) causes a significant increase in synaptic bouton formation in the larval NMJ (4, 5). In contrast, loss-of-expression mutants of the *Drosophila* ortholog of BMPR2 *Wit* exhibit a reduced number of synaptic boutons (11, 12). When one allele of *Wit* is mutated in *dFMR1* mutants (*dFMR1*$^{\Delta 113}$,*Wit*$^{A12/+}$), the bouton number is decreased by ~20% (5), suggesting that the overgrowth of boutons in *dFMR1*$^{\Delta 113/+}$ mutants is mediated in part by augmented *Wit* and its downstream signaling pathway. This finding is consistent with results obtained in the mouse FXS model and in human FXS patients. We first hypothesized that an overgrowth of synaptic boutons at the NMJ alters the crawling activities of larvae. We tested the crawling behavior of 10 larvae on an agarose plate by video recording for 1 min (Fig. 1A) and visually measuring their velocity (Fig. 1B). The velocity of *dFMR1*$^{\Delta 113/+}$ mutants was 62% faster than that of wild-type larvae (Fig. 1B, right), suggesting that an increased number of boutons correlates with the augmented crawling velocity. Similar to *dFMR1*$^{\Delta 113/+}$, other *dFMR1* heterozygous mutants, such as *dFMR1*$^{\Delta 50/+}$ (13, 14) and *dFMR1*$^{3/+}$ (14), also exhibited increased NMJ bouton number and augmented crawling velocity compared to wild-type larvae (Fig. 1C), suggesting that these phenotypes are the result of *dFMR1* mutation. Conversely, the velocity of *Wit*$^{A12/+}$ mutants was 40% slower than that in wild-type larvae (Fig. 1B, right), indicating that the decreased number of boutons correlates with a decreased crawling velocity. The velocity of *dFMR1*$^{\Delta 113/+}$ larvae with a *Wit* mutation (*dFMR1*$^{\Delta 113}$,*Wit*$^{A12/+}$ double mutant) was similar to that of wild-type larvae (Fig. 1B, right), paralleling the reduction in bouton number (5). These results suggest that morphological changes in the neuromuscular synapses in *dFMR1*$^{\Delta 113/+}$ larvae can alter the speed at which they crawl and indicate that the increased velocity in *dFMR1*$^{\Delta 113/+}$ mutants is rescued by a concurrent mutation in *Wit*. The results also indicate that the aberrant synaptic morphology and the crawling activity of *dFMR1*$^{\Delta 113/+}$ and other *dFMR1* mutants are, at least in part, caused by increased Wit abundance and downstream Wit signaling (such as through the LIMK1 pathway) in

presynaptic neurons, in agreement with our observations in the CNS neurons of the mouse FXS model (5).

Reversing bouton number and locomotion phenotype in *dFMR1*$^{D113/+}$ larvae by oral administration of a LIMK1 inhibitor

Our previous study correlated augmented BMPR2 protein amount in FXS animal models and patients with activation of LIMK1, phosphorylation of cofilin, and actin remodeling (5). To investigate whether the LIMK1-cofilin axis is also activated in *dFMR1*$^{\Delta 113/+}$ larvae, we performed immunoblot analysis of phosphorylated Twinstar (P-Tsr), the *Drosophila* ortholog of cofilin, relative to total Tsr (t-Tsr). The relative basal amount of P-Tsr in *dFMR1*$^{\Delta 113/+}$ mutants was 26% greater than that in wild-type larvae (Fig. 2A, mock), indicative of augmented *Drosophila* LIMK (dLIMK) activity in *dFMR1*$^{\Delta 113/+}$ mutants. This finding provided us the opportunity to test whether oral delivery of the LIMK inhibitor LIMKi-3 (LIMK-i) to *dFMR1*$^{\Delta 113/+}$ larvae could inhibit dLIMK activity. Increasing concentrations of LIMK-i (5, 10, or 50 μM) were administered orally to *dFMR1*$^{\Delta 113/+}$ or wild-type third-instar larvae, followed by assessment of the relative P-Tsr amount (Fig. 2A). LIMK-i dose-dependently decreased the relative amount of P-Tsr ultimately to a value similar to mock-treated wild-type larvae (Fig. 2A), indicating that augmented dLIMK activity in *dFMR1*$^{\Delta 113/+}$ was suppressed by oral delivery of LIMK-i. Unlike *dFMR1*$^{\Delta 113/+}$ larvae, the relative amount of P-Tsr in wild-type larvae that received LIMK-i was not affected upon visual assessment of the blots (Fig. 2A), indicating little to no effect on the physiological dLIMK activity.

To examine whether the inhibition of LIMK1 leads to changes in the number of NMJ boutons in *dFMR1*$^{\Delta 113/+}$ larvae, we fed *dFMR1*$^{\Delta 113/+}$ or wild-type larvae increasing concentrations of LIMK-i and analyzed the number of mature synaptic boutons by immunofluorescence staining of the postsynaptic marker discs large 1 (Dlg1) (Fig. 2B, green) and phalloidin (Fig. 2B, red) on M6/M7 muscles in the A3 segment of third-instar larvae. Consistent with previously reported data (4, 5), mock-treated *dFMR1*$^{\Delta 113/+}$ mutants had ~40% more boutons than did mock-treated wild-type larvae (Fig. 2B, graph), and even the lowest concentration(10μM) of LIMK-i used decreased the average number of boutons to a similar number observed in the mock-treated wild-type larvae (96) (Fig. 2B, graph). This result indicates that administration of LIMK-i can reverse the abnormal NMJ bouton phenotype in *dFMR1*$^{\Delta 113/+}$ larvae similarly to the result of the gene dosage reduction of *Wit* (5).

Development of an algorithm to measure the crawling distance of larvae

The change in the NMJ bouton number mirrored by the locomotion behavior in *dFMR1*$^{\Delta 113/+}$ larvae prompted us to use the crawling assay for a screening of drugs to treat conditions associated with abnormal synapse formation, such as FXS and autism (15). To develop a high-throughput drug screen with locomotion velocity as functional readout of NMJ bouton phenotype, we devised a semiautomated analysis of the larval crawling path and distance traveled based on an algorithm we named “LarvaTrack” (see Materials and Methods and text S1). Larva-Track can trace the path of as many as 10 larvae simultaneously (Fig. 3A) while measuring their crawling distance (Fig. 3B), which allows

auto mated calculation of the average velocity (Fig. 3C). Using LarvaTrack to analyze the locomotion videos, we found that the mock-treated *dFMR1*$^{\Delta 113/+}$ mutants traveled ~30% farther than mock-treated wild-type larvae in 60 s (Fig. 3B). The distance traveled by *dFMR1*$^{\Delta 113/+}$ mutants was reduced by treatment with LIMK-i to a value similar to or lower than the distance traveled by mock-treated wild-type larvae (Fig. 3B). The velocity of mock-treated *dFMR1*$^{\Delta 113/+}$ mutants (1.5 ± 0.03 mm/s) was ~20% faster than that of mock-treated wild-type larvae (Fig. 3C). LIMK-i treatment reduced the velocity of *dFMR1*$^{\Delta 113/+}$ larvae, which, to a measure, is similar to that of mock-treated wild-type larvae (Fig. 3C). LIMK-i treatment also decreased the velocity of wild-type larvae to 0.89 ± 0.06 mm/s (Fig. 3C). Furthermore, unlike mock-treated larvae, which crawled from the center to the periphery in a linear fashion, LIMK-i treatment (100 μM) induced frequent turning and circling behavior in both wild-type and *dFMR1*$^{\Delta 113/+}$ larvae (Fig. 3D), which suggests that high doses of LIMK-i cause neurotoxicity. To further confirm the effects of LIMK-i in *dFMR1*$^{\Delta 113/+}$ larvae, we administered LIMK-i to heterozygous (*dFMR1*$^{3/+}$) and transheterozygous (*dFMR1*$^{\Delta 113/3}$) lines of *dFMR1* mutants, as well as to a transgenic line in which small inhibitory RNA (RNAi) against *dFMR1* is expressed in neurons (*dFMR1*^{RNAi}), followed by assessment of the NMJ bouton phenotype and the crawling velocity. Consistent with *dFMR1*$^{\Delta 113/+}$ larvae, *dFMR1*$^{3/+}$, *dFMR1*$^{\Delta 113/3}$, and *dFMR1*^{RNAi} larvae all had greater numbers of boutons and faster velocity compared to wild-type larvae, and inhibition of LIMK activity ameliorated both parameters to amounts similar to wild type (Fig. 3E). Thus, the semiautomated assessment of crawling velocity by LarvaTrack is a sensitive and quantitative assay for monitoring changes in synaptic bouton phenotype in the *Drosophila* FXS model, indicating that this method might be usable as a screening strategy to discover and assess the toxicity of new FXS therapies.

Application of *dFMR1* mutant larval crawling assay to screen drugs for FXS and other disease associated with aberrant dendritic spine phenotype

To test whether the larval crawling velocity assay can be used to screen drugs that ameliorate the abnormal synaptic bouton phenotype in the FXS model, several small molecules were examined. It was previously reported that FMRP bound to its target mRNAs inhibits translation in association with polyribosomes and that derepression of FMRP target mRNAs induced by the ablation of FMRP can be reversed by puromycin, an inhibitor of protein synthesis (16). Administration of puromycin ameliorates the long-term olfactory memory in *dFMR1* mutant *Drosophila* (17). Thus, we tested whether puromycin might reverse the locomotion phenotype in *dFMR1* mutant larvae. Various concentrations of puromycin (0.1, 0.5, or 1 mM) or vehicle (H_2O, “mock”) were administered to third-instar larvae, followed by the locomotion assay (Fig. 4A) and analysis of NMJ boutons (Fig. 4B). Similar to the result of LIMK-i (Fig. 3B), the velocity of mock-treated *dFMR1*$^{\Delta 113/+}$ mutants was ~20% faster than that of mock-treated wild-type larvae (Fig. 4A). The two lower doses (0.1 and 0.5 mM) of puromycin reduced the velocity of *dFMR1*$^{\Delta 113/+}$ larvae to that comparable to mock-treated wild-type larvae (Fig. 4A). At the higher dose (1 mM), the velocity of both wild-type and *dFMR1*$^{\Delta 113/+}$ mutants was severely affected (Fig. 4A). Along with the decrease in locomotion, puromycin caused a dose-dependent decrease in the number of NMJ boutons in *dFMR1* mutants (Fig. 4B). We also tested the effect of two allosteric, highly selective antagonists of LIMK1 and LIMK2 (LIMK1/2), TH251 [LIMK2; median inhibitory

concentration (IC_{50}), 0.003 μM] and TH255 (LIMK2; IC_{50}, 0.039 μM) (18), as well as an inactive analog of TH251 and TH255, called TH263 (Fig. 4C and fig. S1), in *dFMR1*$^{\Delta 113/+}$ or wild-type larvae. Different concentrations (1, 10, or 50 μM) of these compounds were administered through the food, followed by assessment of crawling velocity by LarvaTrack and measurement of the NMJ bouton number (Fig. 4C). Similar to the results of LIMK-i (Figs. 2B and 3C), both active LIMK antagonists (TH251 and TH255) reduced the crawling velocity in *dFMR1*$^{\Delta 113/+}$ in a dose-dependent manner (Fig. 4C and fig. S1). The reduction of crawling velocity was accompanied by a reduced bouton number (Fig. 4C). When the inactive compound (TH263) was administered, neither the locomotion phenotype nor the bouton number of *dFMR1*$^{\Delta 113/+}$ mutants was affected (Fig. 4C), demonstrating the selectivity of the effect of LIMK inhibitors. Neither TH251 nor TH255 exhibited an effect on the crawling velocity or the bouton number in wild-type larvae (Fig. 4C). These results demonstrate that changes in larval locomotion can reflect changes in NMJ bouton number and that the *dFMR1* larvae crawling assay can serve as a screening strategy for compounds that ameliorate synaptic abnormalities. They also support a therapeutic potential of LIMK1 antagonists for FXS.

Reversing behavioral deficits in the mouse FXS model by administration of LIMK inhibitor

To support the therapeutic potential of LIMK1 antagonists for FXS in a mammalian model, we performed behavioral studies in FXS model mice. Our previously reported results show that when *FMR1* homozygous null (*FMR1*-KO) mice were treated with LIMK-i postnatally at postnatal day 1 (P1) and P4, both spine density and the fraction of immature spines in the dentate gyrus (5) and CA3 (fig. S2) were reversed to those observed in vehicle-treated wild-type mice. To examine whether the postnatal inhibition of LIMK1 could ameliorate the *FMR1*-KO cognitive and behavioral deficits, we administered LIMK-i or vehicle (DMSO) to male *FMR1*-KO mice at P1, P4, and 3 months of age, and the mice were subjected to a "repeated open-field test" (rOFT) at 3 to 3.5 months of age. rOFT not only provides a simple assessment of spontaneous locomotion activity and exploratory behavior in a new environment but also monitors habituation to a spatial environment and memory for that environment throughout the test (19). The test mice were given four 5-min sessions in a clear acrylic OFT chamber twice per day over two consecutive days (sessions #1 and #2 on day 1 and sessions #3 and #4 on day 2). On day 16, the mice were retested in the OFT chamber for two more sessions (sessions #5 and #6) to examine their spatial memory. The total number of spontaneous movements, including horizontal (fine or ambulatory movement; total activities) and vertical (rearing) movements, was individually counted by a Flex-Field/Open-Field Photobeam Activity System, and average values of multiple mice are presented (Fig. 5A). The total activities of mock-treated *FMR1*-KO mice reached a plateau on day 2 at session #3 (Fig. 5A, red line), in contrast to mock-treated wild-type mice, which reached a plateau a day earlier at session #2 (Fig. 5A, black line). This result indicates that the *FMR1*-KO mice require a longer period to familiarize with a novel environment compared to control mice. This observation has been previously reported as an indication of memory deficit (20, 21). When *FMR1*-KO mice were treated with LIMK-i (Fig. 5A, blue line), their learning curve became similar to that of mock-treated wild-type mice (Fig. 5A, black), indicating that the LIMK-i treatment improves memory in *FMR1*-KO mice. To measure the behavior of animals placed in an OFT chamber without previous acclimation, we averaged

the total activities at day 1 (sessions #1 and #2) and day 16 (sessions #5 and #6). This analysis revealed that the mock-treated *FMR1*-KO mice exhibited a significantly higher number of total activities compared to mock-treated wild-type mice (Fig. 5B, left), indicating that *FMR1*-KO mice present a hyperactive behavior in a new environment, as reported previously (22–24). Consistently, the mock-treated *FMR1*-KO mice exhibited 2.1-fold higher frequency of rearing behavior compared to mock-treated wild-type littermates (Fig. 5B, right). Compared to mock-treated *FMR1*-KO mice, LIMK-i–treated *FMR1*-KO mice exhibited a reduced number of total activities similar to that in mock-treated wild-type littermates (Fig. 5B, left), suggesting that LIMK-i treatment may be effective in treating hyperactivity and anxiety in *FMR1*-KO mice. No significant difference in total activity or rearing behavior was observed in LIMK-i–treated wild-type mice compared to mock-treated wild-type mice (Fig. 5B). Together, these data suggest that LIMK-i treatment of *FMR1-KO* mice improves memory and reduces hyperactivity, two common characteristics of FXS patients (8). Thus, the results obtained in the *Drosophila* and mouse models of FXS converge in supporting the role of LIMK-i in reversing part of the FXS phenotype. They also support an association between dysregulation of the LIMK1-cofilin pathway and the pathogenesis of FXS. Inhibition of the LIMK1-cofilin or the BMP signaling pathways is, therefore, a potentially promising therapy for the behavioral and cognitive deficits of FXS. Finally, these results validate the semiautomated assessment of the crawling velocity by LarvaTrack as a sensitive and quantitative assay for indirectly monitoring changes in synaptic bouton phenotype in the *Drosophila* FXS model, which could serve as a novel screening strategy for the discovery of FXS therapies.

DISCUSSION

Presynaptic Wit as a critical receptor for the development and function of neuromuscular synapses

In *Drosophila*, glass bottom boat (Gbb), which is produced by the post-synaptic muscle, binds to the presynaptic receptor Wit and plays a critical role in modulating neuromuscular synaptic growth, stability, and function. Upon Gbb binding, Wit forms a heteromeric receptor complex with Thickveins (Tkv) and Saxophone (Sax), which then phospho-rylate Mothers against decapentaplegic (MAD), a *Drosophila* homolog of Smad1/5/8 (25). It has been reported that loss of Spartin, a *Drosophila* homolog of SPG20 that promotes endocytotic degradation of Wit and represses the BMP-Wit signaling pathway, results in an increment of neuromuscular synapses (26). The result with the $dFMR1^{\Delta 113/+}$ mutant is consistent with the Spartin study and confirms the effect of increased Gbb-Wit signal on abnormal synapse development (26). Loss-of-expression mutants of Spartin develop age-dependent and progressive neuronal defects resembling hereditary spastic paraplegia (HSP) (26). Because frameshift mutations in the SPG20 gene cause a form of HSP known as Troyer syndrome (Online Mendelian Inheritance in Man no. 275900) (27), these results underscore the significance of a presynaptic BMP signal finely tuned by multiple regulatory molecules, including SPG20 and FMRP, for proper motor neuron development and function. Beyond the domain of the NMJ, multiple studies reinforce the notion that the correct intensity and spatiotemporal dynamics of the BMP signaling pathway are critical for axon regeneration upon neuronal and glial injury responses after CNS injury (28). Furthermore,

BMP signaling specifies large and fast-transmitting synapses in the auditory system in a process that largely shares homologies with retrograde BMP signaling in *Drosophila* neuromuscular synapses (29). In line with these findings, our results propose an essential role for the FMRP-BMPR2 axis in the development of the neuropathology of patients with FXS.

Limitations of behavioral assays in mice

The major obstacle against the development of drugs for neurodevelopmental and neurodegenerative diseases is the lack of proper animal models that recapitulate the range of intellectual disability and/or cognitive dysfunction found in human patients. The existing, inadequate models also lack quantitative and reproducible assays to examine cognitive phenotypes. The mouse model of FXS exhibits cognitive and behavioral phenotypes that are both consistent and inconsistent with the symptoms of patients with FXS. For example, a frequent FXS trait is a high-anxiety behavior, whereas the *FMR1*-KO mice exhibit lower anxiety–like behaviors in the “light-dark compartment” test (30, 31). Furthermore, the result of the OFT is confusing because the *FMR1*-KO mice tend to spend a longer period in the center. The number of crossings and their velocity are both augmented compared to control mice because of their hyperactivity, but this behavior is interpreted as lower anxiety–like (24, 30, 32, 33). The results of the “elevated plus maze (EPM)” test, which is frequently used to investigate anxiety-like behaviors in FXS mice, exhibit both a decrease (34) and an increase (35) in anxiety. Furthermore, the tests show great variability and, sometimes, opposing outcomes in behavior depending on the genetic background of the mice, for example, FVB versus C57BL/6J (8). Considering the variability and lack of reproducibility of behavioral test results in *FMR1*-KO mice, as well as the concerns of animal welfare and the cost of husbandry, there is a strong need for an animal model and phenotypic readout to screen for FXS drugs.

Advantages of the *Drosophila* FXS model

There are multiple advantages of the *Drosophila* FXS model over the rodent models. Flies are invertebrates, which are inexpensive and easily cared for. They have a shorter life span and produce numerous externally laid embryos than rodent models. Their genome is small, minimally redundant, and easy to genetically manipulate in a tissue-specific manner (36, 37). It is easy to orally administer drugs to larvae by adding compounds to the *Drosophila* medium Formula 4–24 (Carolina Biological Supply Company). Previously, small molecules had to be delivered through conventional fly food that requires boiling followed by the addition of propionic acid, which disables the effect of heat- or acid-sensitive molecules. The use of Formula 4–24, which can be dissolved in water at room temperature and does not require exposure to high temperature nor addition of acid, expands the range of molecules that can be delivered to larvae without loss of activity.

Drosophila has contributed extensively to the discovery and validation of drug targets, as well as to the mechanistic understanding of their genetic cause (4, 14). In the context of FXS studies, it has been reported that *dFMR1* adult mutant flies exhibit defects in learning/memory assays, such as Pavlovian olfactory association (17) and courtship conditioning (38). These behavioral abnormalities can be restored by various compounds known to target

different FMRP targets, including protein synthesis inhibitors, such as puromycin and cycloheximide (17), the metabotropic glutamate receptor 5 antagonist MPEP (38), γ-aminobutyric acid agonists (39, 40), phosphodiesterase-4 inhibitor (41), and glycogensynthasekinase3inhibitor (38,42).Our study demonstrates that several d*FMR1* mutant larvae exhibit an abnormally high number of NMJ synaptic boutons that correlate with their locomotion abnormality. Both are reversed by LIMK-i treatment, similarly to the effect of this drug in the *FMR1*-KO mouse. Thus, we propose the crawling assay in *dFMR1* mutant *Dro-sophila* larvae as a rapid, quantitative, and reproducible preclinical screening strategy for potential FXS therapies that is alternative to behavioral tests using *dFMR1* adult mutant flies or vertebrate FXS models. To facilitate the transition to a high-throughput screen of FXS drugs, the current assay will benefit from an improvement in the number of larvae that can be simultaneously assessed and in the robustness of the phenotype of $dFMR1^{\Delta 113/+}$ mutants.

Larval crawling assay as a functional readout for the change in NMJ boutons

Larval locomotion abnormalities are described in *Drosophila* models of CNS diseases, such as Alzheimer's (43, 44) and Huntington's (45, 46). It has been reported that a different strain of *dFMR1* mutant *Drosophila* larvae ($dFMR1^{4}$) (47) exhibits frequent turnings compared to wild-type larvae (44, 48). We observed that various *dFMR1* mutants, including $dFMR1^{\Delta 113/+}$, $dFMR1^{\Delta 50/+}$, $dFMR1^{3/+}$, and $dFMR1^{\Delta 113/3}$, as well as the *dFMR1*-RNAi line, crawled from the center to the periphery in a linear manner with an enhanced velocity compared to wild-type larvae. We speculate that this discrepancy might be due to the different nature of the mutations. For example, $dFMR1^{\Delta 113}$ harbors a deletion of the first three exons of the *dFMR1* gene, including exon 3 that contains the translation initiation methionine (4). Consequently, the $dFMR1^{\Delta 113}$ allele results in a loss of dFMRP (4). On the contrary, the $dFMR1^{4}$ allele has a replacement of amino acid 289 with a stop codon; hence, it expresses a partial dFMRP missing the C terminus (47). Furthermore, in the process of creating the $dFMR1^{4}$ mutant, a Gal4-binding site was inserted into the first intron between exons 1 and 2 of the *dFMR1* gene to overexpress a truncated dFMRP upon coexpression of Gal4 transcription factor (47). These differences might explain the distinct larval crawling behavior of the $dFMR1^{\Delta 113}$ and $dFMR1^{4}$ mutants. The homozygous $dFMR1^{\Delta 50}$ (13, 14) and homozygous $dFMR1^{3}$ mutants (14) are viable and develop into adulthood similarly to the homozygous $dFMR1^{4}$ mutant (47, 48). The homozygous $dFMR1^{\Delta 50}$and homozygous$dFMR1^{3}$ mutants exhibited frequent turns in the locomotion assay (fig. S3) similar to the previous study of the homozygous $dFMR1^{4}$ mutant (48). The velocity of $dFMR1^{3}$ and $dFMR1^{\Delta 50}$ homozygous mutants was slower than wild-type, presumably because of the frequent changes of direction, unlike the transheterozygous $dFMR1^{\Delta 113/3}$ mutant, which crawled in a linear fashion with an augmented velocity. We speculate that the turning phenotype observed in the homozygous mutants is due to complete loss of dFMRP, affecting the CNS neurons. FMRP activity has already been shown to be important for CNS neuron development and function in *Drosophila* (4, 49–51).

Performing the locomotion assay with larvae instead of adults is beneficial as they present an accessible, anatomically simple, and well-described peripheral nervous system (for example, NMJ boutons), which allows the molecular and biochemical assessment of the

mechanism underlying the locomotion dysfunction and the therapeutic effects of drugs (52). For chemical screens of known pathways or targets, the NMJ synapses of larvae that exhibit an altered crawling phenotype should be subjected to synaptic bouton phenotype analysis as well as biochemical investigation to rapidly validate the “on-target” and eliminate the “off-target” effects of the candidate molecules. Sinadinos *et al*. (53) previously proposed a *Drosophila* larvae locomotion assay as a way to screen drugs for neurodegenerative diseases, such as Alzheimer’s disease. They subjected *Drosophila* larvae expressing the human three-repeat tau gene in motor neurons to crawling assays, such as a five-lane assay and a four-plate open-field assay, video-recorded the locomotion with an Ikegami digital video camera and a 5-mm digital video camera lens, and analyzed locomotion using EthoVision 3.0 software (53). In comparison, the advantage of our strategy is that the assay does not require specialized equipment, but a common video recording device, such as an iPhone camera, and an algorithm that is accessible and free to the scientific community. Furthermore, our system can simultaneously track and assess the crawling activities of multiple larvae through the open-access algorithm LarvaTrack, which we developed to trace and measure larval crawling activity. We have successfully simultaneously assessed up to 15 larvae using a 15-cm agarose plate. The method can be easily adapted to a larger number of larvae by using a larger agarose plate to avoid larvae to cross paths during crawling. Thus, our semiautomated assay of locomotion behavior can allow the higher-throughput assay that is essential for the screen of candidate molecules. In conclusion, activation of the FMRP–BMPR2 axis plays a role in synaptic abnormalities in both mouse and *Drosophila* models of FXS. The larval crawling assay is an easy, fast, and well-suited medium-throughput screen for genetic or chemical modulators of locomotion dysfunction in the *Drosophila* FXS model, which can be further evaluated in cognitive and behavioral tests using mammalian FXS models.

MATERIALS AND METHODS

Chemicals and antibodies

LIMK-i (Tocris Bioscience) and puromycin (Clontech) were dissolved in DMSO (final stock concentration, 100 mM) and water (final stock concentration, 100 mM), respectively, and administered to mice or *Drosophila*. LIMK allosteric antagonists (TH251 and TH255) were synthesized as previously reported (18). The synthesis of the inactive control compound (TH263) is described in text S2. All the compounds (TH251, TH255, and TH263) were dissolved in DMSO (final stock concentration, 10 mM) and administered to *Drosophila*. We used antibodies for phosphorylated cofilin (SC-12912-R, Santa Cruz Biotechnology), *Drosophila* Twinstar (a gift from T. Uemura) (54), actin (AC-15, Thermo Scientific), and Dlg1 (4F3, Developmental Studies Hybridoma Bank). Alexa Fluor 488–conjugated secondary antibody against mouse immunoglobulin G (IgG) and Alexa Fluor 568–conjugated phalloidin (A12380, Life Technologies) were also used.

Drosophila lines

The mutant lines carrying the Wit^{A12}, $dFMR1^{\Delta 113M}$, $dFMR1^{\Delta 50M}$, and *UAS-dFMR1 RNAi* (Bloomington *Drosophila* Stock Center ID #35200) alleles were obtained from the Bloomington *Drosophila* Stock Center (http://flybase.org/reports/FBal0131035.html). The $dFMR1^{3}$ and $elav^{[C155]}$-Gal4 lines were obtained from T. A. Jongens and Y. N. Jan,

respectively. To obtain the *Wit*$^{A12/+}$, *dFMR1*$^{\Delta 113/+}$, and *dFMR1*$^{\Delta 113}$,*Wit*$^{A12/+}$, *dFMR1*$^{\Delta 50/+}$, and *dFMR1*$^{3/+}$ third-instar larvae, the mutant flies were crossed to the *w*^{1118} line. To obtain *dFMR1*$^{\Delta 113/3}$ third-instar larvae, *dFMR1*$^{\Delta 113}$/*TM6B, Tb* and *dFmr1*^{3}/*TM6C, Tb, Sb* flies were crossed. The wild-type *Drosophila* melanogaster *w*^{1118} line was used as a control. *Drosophila* strains were cultured at 25°C in 50 to 70% humidity in a 12 hour/12 hour light/dark cycle, on cornmeal-sucrose-yeast medium supplemented with the mold inhibitor methylparaben and autoclaved.

To express *UAS-dFMR1 RNAi* in the neuron, *UAS-dFMR1 RNAi* female flies were crossed with *elav-Gal4* male flies, kept at 16°C until the first and second larval stages, and incubated at 29°C for 1 day. As a control, *w*^{1118} female flies were crossed with *elav-Gal4* male flies and kept as the RNAi line. The third-instar female larvae were used for analysis.

Oral administration of drugs to *Drosophila* larvae

Distilled water (20 ml) at room temperature was added to two measuring cups of the instant *Drosophila* medium Formula 4–24 (Carolina Biological Supply Company) into the culture bottle. LIMK-i in DMSO or puromycin in water was placed on the formula and mixed well, and the formula was brought to the final concentration by addition of 10 ml of water at room temperature. Ten female and 5 male flies were put in the bottle with LIMK-i formula to set up mating. After 5 to 7 days, third-instar larvae were subjected to the crawling assay and the immunoblot analysis.

Immunoblot analysis

Third-instar larvae were lysed in lysis buffer (tris-buffered saline containing 1% NP-40, 1 μM NaF, and 1 mM EDTA) and incubated for 1 hour at 4°C. Lysed samples were separated by SDS–polyacrylamide gel electrophoresis, transferred to a nitrocellulose membrane (Millipore), immunoblotted with antibodies, and visualized using the LI-COR imaging system.

Larva immunofluorescence and image quantitation

Wandering late third-instar larvae were dissected for NMJ phenotype analysis. Briefly, the tissue was fixed with 8% formaldehyde in phosphate-buffered saline (PBS) for 10 min, washed with PBT (PBS containing 0.1% Triton X-100), and blocked with 5% normal donkey serum in PBT for 1 hour at room temperate. The larvae were incubated with Dlg1 antibody overnight at 4°C, followed by incubation with Alexa Fluor 488–conjugated secondary antibody against mouse IgG and Alexa Fluor 568–conjugated phalloidin. Confocal images were acquired using a point scanning confocal microscope (Leica). Images for quantification of NMJ bouton number on muscles 6 and 7 at segment 3 were produced by projection of z-sections using the ImageJ software blindly.

Larval crawling assay

Larval crawling abilities were examined as reported previously (55). Briefly, third-instar larvae (n = 10) were placed on the center of a 15-cm petri dish containing 2% agarose, and their crawling behavior was digitally recorded for 1 min using an iPhone 4S (Apple) in QuickTime movie (MOV) format. The videos were analyzed either manually or

computationally. For manual analysis of crawling, the relative crawling distance every 15 s was quantitated by counting the number of concentric lines crossed, which was converted to the definitive distance (in millimeters). For the computational analysis, the relative crawling distance of each individual larva was quantitated on the basis of the crawling path traced by the LarvaTrack algorithm (https://github.com/plredmond/ larva-tracker), as described below. The position of each larva was recorded on most frames, and the cumulative distance (in millimeters) was computed for four 15-s intervals. The velocity was calculated by determining the average speed from 15 to 45 s. Beginning and end of the path were excluded because the larvae did not move the first 10 s and some of them reached the edge of the petri dish by the last 10 s.

LarvaTrack algorithm

LarvaTrack takes a video satisfying the following constraints. A time-lapse video was taken by a motionless camera at two frames per second (fps) and encoded via wall-clock time for playback at 30 fps. The total length of the video was 4 s, or 120 frames, representing 60-s wall-clock time. The camera was positioned motionless for the duration of the video. A 15-cm petri dish filled the narrow dimension of the frame. A coin (in this case, a penny measuring 19.05 mm), was present in the frame for scale. The background observable through the petri dish was a solid blue color distinct from the color of the larva.

We constructed a deterministic multiple-point object tracker in the following way. We detected larva locations (“detected location”) in each video frame with the OpenCV blob detector. We updated those larva locations (“flowed location”) in each frame with data from the following frame using the OpenCV optical-flow algorithm. Finally, for each successive pair of frames, we assigned some flowed locations from the earlier frame to some detected locations in the later frame. For this, we applied a variation of the Gale-Shapley stable matching algorithm (www.jstor.org/stable/2312726). The resulting digitized larval paths were used to compute average velocity and distance traveled over four 15-s intervals. For additional resources and code, see the Supplementary Materials (text S1 and fig. S4) and the online repository (https://github.com/ plredmond/larva-tracker).

FXS mouse model

B6.129P2-*FMR1*^{tm1Cgr}/J mice were maintained under standard conditions. To obtain *FMR1* knockout littermates, *FMR1* heterozygous female and hemizygous male mice were mated, and wild-type and knockout (*FMR1*$^{-/-}$) male mice were used. Genotyping was performed following the Jackson Laboratory protocol.

Mouse behavior analyses

LIMK-i or DMSO was administered to B6.129P2-*FMR1*^{tm1Cgr}/J and littermate wild-type mice by intracerebroventricular injection at P1 and P4 (20 μg per pup) and by intraperitoneal injection twice at about 3 months of age (80 mg/kg) and again after 2 weeks. Two weeks after the final injection, the mice were examined by the rOFT at the Behavioral Core Facility of the Gladstone Institute (19). Briefly, mice were transferred to the testing room 60 min before testing to acclimate them to the testing conditions under normal lighting. For the rOFT, mice were given four 5-min sessions in a clear acrylic OFT chamber (41 × 41 × 30

cm) twice per day, once in the morning and once in the afternoon over two consecutive days (sessions #1 and #2 on the first day and sessions #3 and #4 on the second day). After these sessions, the mice were retested after 14 days in the OFT chamber for two more 5-min sessions separated by 3 to 4 hours (sessions #5 and #6). Spontaneous locomotion activity at each session was measured in an OFT chamber with two 16 × 16 photobeam arrays that detect horizontal (fine or ambulatory movement) and vertical (rearing) movements, which is also known as a Flex-Field/Open-Field Photobeam Activity System (San Diego Instruments). Fine movements were defined as having broken less than three photobeams. Ambulatory movements were defined as having broken more than three photobeams. Ambulatory movements were interpreted as walking, whereas fine movements accounted for grooming or perhaps stretching. Total activities were measured by calculating ambulatory and fine movements. Locomotion and exploratory activities were monitored by measuring the total activity and the rearing movement throughout the six sessions, respectively. This study was performed in strict accordance with the recommendations in the *Guide for the Care and Use of Laboratory Animals* of the National Institutes of Health. All of the animals were handled according to approved Institutional Animal Care and Use Committee protocols (AN108100) of University of California, San Francisco (UCSF). The protocol was approved by the Committee on the Ethics of Animal Experiments of UCSF and Gladstone Institute.

Statistical analysis

Statistical analysis was performed using the GraphPad Prism 7.0 package and reviewed by M. Nojima at the University of Tokyo. Statistical test and significance are denoted in the figure legends. Statistical significance is denoted as described within the figure legends.

Supplementary Material

Refer to Web version on PubMed Central for supplementary material.

Acknowledgments

We thank M. Gill and the Gladstone Institute Behavioral Core Facility staff members for mouse behavioral analysis; T. A. Jongens (University of Pennsylvania) for *dFmr1*^{3}*/TM6C, Tb, Sb* fly stock; Y. N. Jan (UCSF) for *elav*$^{[C155]}$-Gal4 fly stock; T. Uemura (Kyoto University) for the antibody against Twinstar; and H. Li (Airware) and J. A. Trono (Saint Michael's College) for advice in writing the algorithm. We also want to thank M. Nojima for the statistical analysis and S. Liu and S. Manghise for the technical support.

Funding: R.K. is a recipient of a fellowship from Japan Society for the Promotion of Science. This work was supported by grants from the NIH (HL093154 and HL108317) to A.H. and the Program for Breakthrough Biomedical Research to R.K. S.K. is grateful for support by the Structural Genomics Consortium, a registered charity (no. 1097737) that receives funds from AbbVie, Bayer Pharma AG, Boehringer Ingelheim, Canada Foundation for Innovation, Eshelman Institute for Innovation, Genome Canada through Ontario Genomics Institute, Janssen, Merck & Co., Novartis Pharma AG, Ontario Ministry of Economic Development and Innovation, Pfizer, São Paulo Research Foundation (FAPESP), Takeda, the Centre of Excellence Macromolecular Complexes at Frankfurt University, and the Wellcome Trust.

REFERENCES AND NOTES

1. Richter JD, Bassell GJ, Klann E. Dysregulation and restoration of translational homeostasis in fragile X syndrome. Nat Rev Neurosci. 2015; 16:595–605. [PubMed: 26350240]
2. Saldarriaga W, Tassone F, González-Teshima LY, Forero-Forero JV, Ayala-Zapata S, Hagerman R. Fragile X syndrome. Colomb Med. 2014; 45:190–198. [PubMed: 25767309]

3. Darnell JC, Klann E. The translation of translational control by FMRP: Therapeutic targets for FXS. Nat Neurosci. 2013; 16:1530–1536. [PubMed: 23584741]
4. Zhang YQ, Bailey AM, Matthies HJG, Renden RB, Smith MA, Speese SD, Rubin GM, Broadie K. *Drosophila* fragile X-related gene regulates the MAP1B homolog Futsch to control synaptic structure and function. Cell. 2001; 107:591–603. [PubMed: 11733059]
5. Kashima R, Roy S, Ascano M, Martinez-Cerdeno V, Ariza-Torres J, Kim S, Louie L, Lu Y, Leyton P, Bloch KD, Kornberg TB, Hagerman PJ, Hagerman R, Lagna G, Hata A. Augmented noncanonical BMP type II receptor signaling mediates the synaptic abnormality of fragile X syndrome. Sci Signal. 2016; 9:ra58. [PubMed: 27273096]
6. Comery TA, Harris JB, Willems PJ, Oostra BA, Irwin SA, Weiler IJ, Greenough WT. Abnormal dendritic spines in fragile X knockout mice: Maturation and pruning deficits. Proc Natl Acad Sci USA. 1997; 94:5401–5404. [PubMed: 9144249]
7. Till SM, Asiminas A, Jackson AD, Katsanevaki D, Barnes SA, Osterweil EK, Bear MF, Chattarji S, Wood ER, Wyllie DJA, Kind PC. Conserved hippocampal cellular pathophysiology but distinct behavioural deficits in a new rat model of FXS. Hum Mol Genet. 2015; 24:5977–5984. [PubMed: 26243794]
8. Santos AR, Kanellopoulos AK, Bagni C. Learning and behavioral deficits associated with the absence of the fragile X mental retardation protein: What a fly and mouse model can teach us. Learn Mem. 2014; 21:543–555. [PubMed: 25227249]
9. Tauber JM, Vanlandingham PA, Zhang B. Elevated levels of the vesicular monoamine transporter and a novel repetitive behavior in the *Drosophila* model of fragile X syndrome. PLOS ONE. 2011; 6:e27100. [PubMed: 22087250]
10. Zhang J, Fang Z, Jud C, Vansteensel MJ, Kaasik K, Lee CC, Albrecht U, Tamanini F, Meijer JH, Oostra BA, Nelson DL. Fragile X-related proteins regulate mammalian circadian behavioral rhythms. Am J Hum Genet. 2008; 83:43–52. [PubMed: 18589395]
11. Aberle H, Haghighi AP, Fetter RD, McCabe BD, Magalhães TR, Goodman CS. *wishful thinking* encodes a BMP type II receptor that regulates synaptic growth in. Drosophila Neuron. 2002; 33:545–558. [PubMed: 11856529]
12. Marqués G, Bao H, Haerry TE, Shimell MJ, Duchek P, Zhang B, O'Connor MB. The *Drosophila* BMP type II receptor Wishful Thinking regulates neuromuscular synapse morphology and function. Neuron. 2002; 33:529–543. [PubMed: 11856528]
13. Bozzetti MP, Specchia V, Cattenoz PB, Laneve P, Geusa A, Sahin HB, Di Tommaso S, Friscini A, Massari S, Diebold C, Giangrande A. The *Drosophila* fragile X mental retardation protein participates in the piRNA pathway. J Cell Sci. 2015; 128:2070–2084. [PubMed: 25908854]
14. Pan L, Zhang YQ, Woodruff E, Broadie K. The *Drosophila* fragile X gene negatively regulates neuronal elaboration and synaptic differentiation. Curr Biol. 2004; 14:1863–1870. [PubMed: 15498496]
15. Doll CA, Broadie K. Impaired activity-dependent neural circuit assembly and refinement in autism spectrum disorder genetic models. Front Cell Neurosci. 2014; 8:30. [PubMed: 24570656]
16. Stefani G, Fraser CE, Darnell JC, Darnell RB. Fragile X mental retardation protein is associated with translating polyribosomes in neuronal cells. J Neurosci. 2004; 24:7272–7276. [PubMed: 15317853]
17. Bolduc FV, Bell K, Cox H, Broadie KS, Tully T. Excess protein synthesis in *Drosophila* fragile X mutants impairs long-term memory. Nat Neurosci. 2008; 11:1143–1145. [PubMed: 18776892]
18. Goodwin NC, Cianchetta G, Burgoon HA, Healy J, Mabon R, Strobel ED, Allen J, Wang S, Hamman BD, Rawlins DB. Discovery of a type III inhibitor of LIM kinase 2 that binds in a DFG-out conformation. ACS Med Chem Lett. 2015; 6:53–57. [PubMed: 25589930]
19. Sanchez PE, Zhu L, Verret L, Vossel KA, Orr AG, Cirrito JR, Devidze N, Ho K, Yu GQ, Palop JJ, Mucke L. Levetiracetam suppresses neuronal network dysfunction and reverses synaptic and cognitive deficits in an Alzheimer's disease model. Proc Natl Acad Sci USA. 2012; 109:E2895–E2903. [PubMed: 22869752]
20. Ventura R, Pascucci T, Catania MV, Musumeci SA, Puglisi-Allegra S. Object recognition impairment in Fmr1 knockout mice is reversed by amphetamine: Involvement of dopamine in the medial prefrontal cortex. Behav Pharmacol. 2004; 15:433–442. [PubMed: 15343070]

21. Bhattacharya A, Kaphzan H, Alvarez-Dieppa AC, Murphy JP, Pierre P, Klann E. Genetic removal of p70 S6 kinase 1 corrects molecular, synaptic, and behavioral phenotypes in fragile X syndrome mice. Neuron. 2012; 76:325–337. [PubMed: 23083736]
22. Liu ZH, Chuang DM, Smith CB. Lithium ameliorates phenotypic deficits in a mouse model of fragile X syndrome. Int J Neuropsychopharmacol. 2011; 14:618–630. [PubMed: 20497624]
23. Michalon A, Sidorov M, Ballard TM, Ozmen L, Spooren W, Wettstein JG, Jaeschke G, Bear MF, Lindemann L. Chronic pharmacological mGlu5 inhibition corrects fragile X in adult mice. Neuron. 2012; 74:49–56. [PubMed: 22500629]
24. Olmos-Serrano JL, Corbin JG, Burns MP. The $GABA_A$ receptor agonist THIP ameliorates specific behavioral deficits in the mouse model of fragile X syndrome. Dev Neurosci. 2011; 33:395–403. [PubMed: 22067669]
25. Friedman SH, Dani N, Rushton E, Broadie K. Fragile X mental retardation protein regulates trans-synaptic signaling in *Drosophila*. Dis Model Mech. 2013; 6:1400–1413. [PubMed: 24046358]
26. Nahm M, Lee MJ, Parkinson W, Lee M, Kim H, Kim YJ, Kim S, Cho YS, Min BM, Bae YC, Broadie K, Lee S. Spartin regulates synaptic growth and neuronal survival by inhibiting BMP-mediated microtubule stabilization. Neuron. 2013; 77:680–695. [PubMed: 23439121]
27. Patel H, Cross H, Proukakis C, Hershberger R, Bork P, Ciccarelli FD, Patton MA, McKusick VA, Crosby AH. *SPG20* is mutated in Troyer syndrome, an hereditary spastic paraplegia. Nat Genet. 2002; 31:347–348. [PubMed: 12134148]
28. Zhong J, Zou H. BMP signaling in axon regeneration. Curr Opin Neurobiol. 2014; 27:127–134. [PubMed: 24713578]
29. Xiao L, Michalski N, Kronander E, Gjoni E, Genoud C, Knott G, Schneggenburger R. BMP signaling specifies the development of a large and fast CNS synapse. Nat Neurosci. 2013; 16:856–864. [PubMed: 23708139]
30. Peier AM, McIlwain KL, Kenneson A, Warren ST, Paylor R, Nelson DL. (Over) correction of FMR1 deficiency with YAC transgenics: Behavioral and physical features. Hum Mol Genet. 2000; 9:1145–1159. [PubMed: 10767339]
31. Veeraragavan S, Graham D, Bui N, Yuva-Paylor LA, Wess J, Paylor R. Genetic reduction of muscarinic M_4 receptor modulates analgesic response and acoustic startle response in a mouse model of fragile X syndrome (FXS). Behav Brain Res. 2012; 228:1–8. [PubMed: 22123412]
32. Chen L, Toth M. Fragile X mice develop sensory hyperreactivity to auditory stimuli. Neuroscience. 2001; 103:1043–1050. [PubMed: 11301211]
33. Restivo L, Ferrari F, Passino E, Sgobio C, Bock J, Oostra BA, Bagni C, Ammassari-Teule M. Enriched environment promotes behavioral and morphological recovery in a mouse model for the fragile X syndrome. Proc Natl Acad Sci USA. 2005; 102:11557–11562. [PubMed: 16076950]
34. Yuskaitis CJ, Mines MA, King MK, Sweatt JD, Miller CA, Jope RS. Lithium ameliorates altered glycogen synthase kinase-3 and behavior in a mouse model of fragile X syndrome. Biochem Pharmacol. 2010; 79:632–646. [PubMed: 19799873]
35. Bilousova TV, Dansie L, Ngo M, Aye J, Charles JR, Ethell DW, Ethell IM. Minocycline promotes dendritic spine maturation and improves behavioural performance in the fragile X mouse model. J Med Genet. 2009; 46:94–102. [PubMed: 18835858]
36. Mohr SE, Smith JA, Shamu CE, Neumüller RA, Perrimon N. RNAi screening comes of age: Improved techniques and complementary approaches. Nat Rev Mol Cell Biol. 2014; 15:591–600. [PubMed: 25145850]
37. Hirth F. *Drosophila melanogaster* in the study of human neurodegeneration. CNS Neurol Disord Drug Targets. 2010; 9:504–523. [PubMed: 20522007]
38. McBride SMJ, Choi CH, Wang Y, Liebelt D, Braunstein E, Ferreiro D, Sehgal A, Siwicki KK, Dockendorff TC, Nguyen HT, McDonald TV, Jongens TA. Pharmacological rescue of synaptic plasticity, courtship behavior, and mushroom body defects in a *Drosophila* model of fragile X syndrome. Neuron. 2005; 45:753–764. [PubMed: 15748850]
39. Chang S, Bray SM, Li Z, Zarnescu DC, He C, Jin P, Warren ST. Identification of small molecules rescuing fragile X syndrome phenotypes in *Drosophila*. Nat Chem Biol. 2008; 4:256–263. [PubMed: 18327252]

40. Idrissi, A El, Boukarrou, L., Dokin, C., Brown, WT. Taurine improves congestive functions in a mouse model of fragile X syndrome. Adv Exp Med Biol. 2009; 643:191–198. [PubMed: 19239149]
41. Kanellopoulos AK, Semelidou O, Kotini AG, Anezaki M, Skoulakis EMC. Learning and memory deficits consequent to reduction of the fragile X mental retardation protein result from metabotropic glutamate receptor-mediated inhibition of cAMP signaling in *Drosophila*. J Neurosci. 2012; 32:13111–13124. [PubMed: 22993428]
42. Mines MA, Yuskaitis CJ, King MK, Beurel E, Jope RS. GSK3 influences social preference and anxiety-related behaviors during social interaction in a mouse model of fragile X syndrome and autism. PLOS ONE. 2010; 5:e9706. [PubMed: 20300527]
43. Folwell J, Cowan CM, Ubhi KK, Shiabh H, Newman TA, Shepherd D, Mudher A. Aβ exacerbates the neuronal dysfunction caused by human tau expression in a *Drosophila* model of Alzheimer's disease. Exp Neurol. 2010; 223:401–409. [PubMed: 19782075]
44. Günther MN, Nettesheim G, Shubeita GT. Quantifying and predicting *Drosophila* larvae crawling phenotypes. Sci Rep. 2016; 6:27972. [PubMed: 27323901]
45. Boudreau RL, McBride JL, Martins I, Shen S, Xing Y, Carter BJ, Davidson BL. Nonallele-specific silencing of mutant and wild-type huntingtin demonstrates therapeutic efficacy in Huntington's disease mice. Mol Ther. 2009; 17:1053–1063. [PubMed: 19240687]
46. Sinadinos C, Burbidge-King T, Soh D, Thompson LM, Marsh JL, Wyttenbach A, Mudher AK. Live axonal transport disruption by mutant huntingtin fragments in *Drosophila* motor neuron axons. Neurobiol Dis. 2009; 34:389–395. [PubMed: 19268537]
47. Lee A, Li W, Xu K, Bogert BA, Su K, Gao FB. Control of dendritic development by the *Drosophila fragile X-related* gene involves the small GTPase Rac1. Development. 2003; 130:5543–5552. [PubMed: 14530299]
48. Xu K, Bogert BA, Li W, Su K, Lee A, Gao FB. The *fragile X-related* gene affects the crawling behavior of *Drosophila* larvae by regulating the mRNA level of the DEG/ENaC protein pickpocket1. Curr Biol. 2004; 14:1025–1034. [PubMed: 15202995]
49. Michel CI, Kraft R, Restifo LL. Defective neuronal development in the mushroom bodies of *Drosophila fragile X mental retardation 1* mutants. J Neurosci. 2004; 24:5798–5809. [PubMed: 15215302]
50. Dockendorff TC, Su HS, McBride SMJ, Yang Z, Choi CH, Siwicki KK, Sehgal A, Jongens TA. *Drosophila* lacking *dfmr1* activity show defects in circadian output and fail to maintain courtship interest. Neuron. 2002; 34:973–984. [PubMed: 12086644]
51. Morales J, Hiesinger PR, Schroeder AJ, Kume K, Verstreken P, Jackson FR, Nelson DL, Hassan BA. *Drosophila* fragile X protein, DFXR, regulates neuronal morphology and function in the brain. Neuron. 2002; 34:961–972. [PubMed: 12086643]
52. Gramates LS, Budnik V. Assembly and maturation of the *Drosophila* larval neuromuscular junction. Int Rev Neurobiol. 1999; 43:93–117. [PubMed: 10218156]
53. Sinadinos C, Cowan CM, Wyttenbach A, Mudher A. Increased throughput assays of locomotor dysfunction in *Drosophila* larvae. J Neurosci Methods. 2012; 203:325–334. [PubMed: 21925540]
54. Niwa R, Nagata-Ohashi K, Takeichi M, Mizuno K, Uemura T. Control of actin reorganization by Slingshot, a family of phosphatases that dephosphorylate ADF/cofilin. Cell. 2002; 108:233–246. [PubMed: 11832213]
55. Nichols CD, Becnel J, Pandey UB. Methods to assay *Drosophila* behavior. J Vis Exp. 2012; 2012:e3795.
56. Yuen HK, Princen J, Illingworth J, Kittler J. Comparative-study of hough transform methods for circle finding. Image Vis Comput. 1990; 8:71–77.

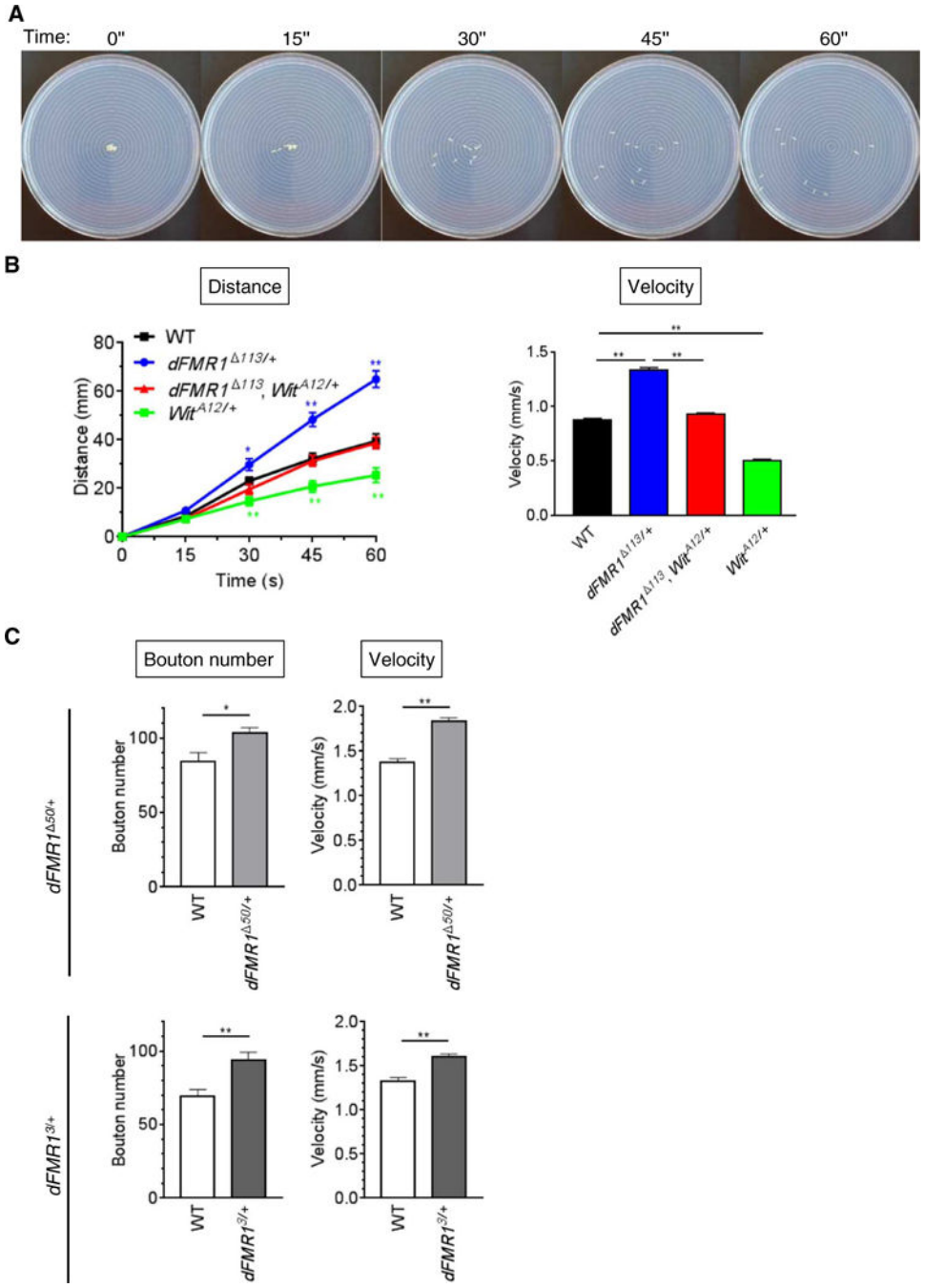

Fig. 1. Increased larval locomotion activity of the *Drosophila* FXS model

(**A**) Representative images of the larval crawling assay performed on an agarose plate. (**B**) The larval crawling assay of wild-type (WT), $dFMR1^{\Delta 113/+}$, $Wit^{A12/+}$, and $dFMR1^{\Delta 113}$, $Wit^{A12/+}$ larvae (n = 10 each) was performed by video-recording the crawling behavior for 1 min, followed by measuring the distance that the larvae traveled every 15 s (bottom left). The velocity was calculated on the basis of the plot shown in (A) (bottom right). Data are means ± SEM. $^{**}P < 0.01$, by analysis of variance (ANOVA) with post hoc Tukey's test. (**C**) The NMJ bouton number at muscle 6/7 in segment A3 and the larval crawling velocity of

WT, *dFMR1*$^{\Delta 50/+}$, and *dFMR1*$^{3/+}$ third-instar larvae were assessed. Data are means ± SEM of 19 to 20 independent images. The crawling velocity of 10 larvae was analyzed simultaneously and repeated four times. Data are means ± SEM. *$P < 0.05$ and **$P < 0.01$, by *t* test.

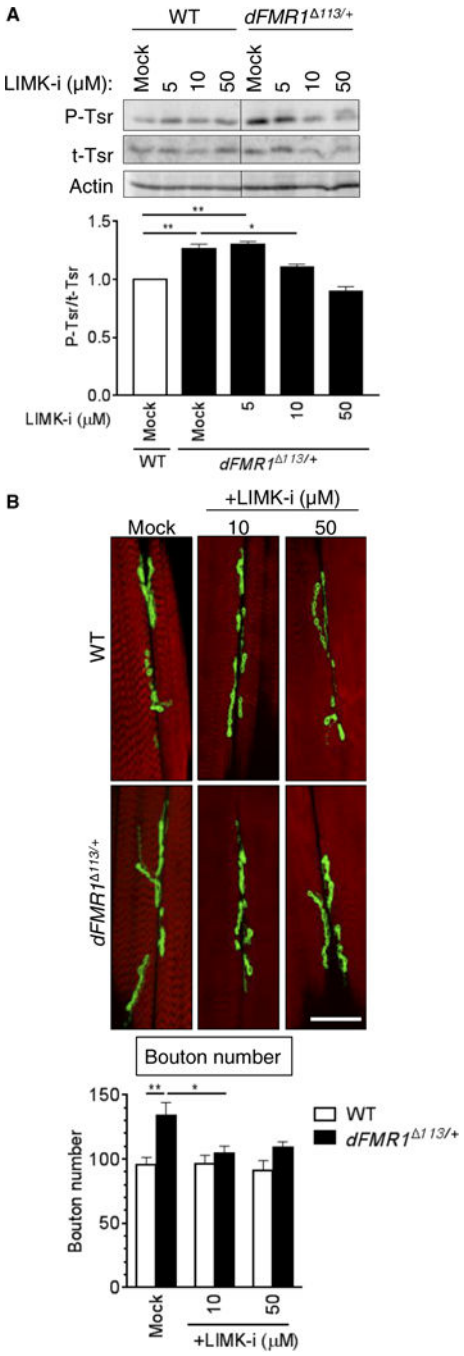

Fig. 2. Inhibition of LIMK1 restores the number of boutons as well as the crawling behavior in *dFMR1*$^{D113/+}$ larvae

(**A**) Third-instar WT or *dFMR1*$^{\Delta 113/+}$ larvae were fed with food containing different doses of LIMK-i as indicated, and total larval lysates were subjected to immunoblot analysis of P-Tsr, t-Tsr, and actin (loading control). The immunoblot result (top) is shown as the relative P-Tsr/t-Tsr ratio, when the P-Tsr/t-Tsr ratio of mock-treated WT larvae is 1 (bottom). Data are means ± SEM of five independent immunoblots. *$P < 0.05$ and **$P < 0.01$, by ANOVA with post hoc Tukey's test. (**B**) WT or *dFMR1*$^{\Delta 113/+}$ mutant third-instar larvae were treated

with increasing doses of LIMK-i, as indicated, and boutons and muscle were stained with Dlg1 antibody (green) and Alexa Fluor 568–conjugated phalloidin (red), respectively. Representative confocal microscopy images of muscle 6/7 in segment A3 are presented (top). Scale bar, 25 μm. Data are means ± SEM of 9 to 16 independent images (bottom). *$P < 0.05$ and **$P < 0.01$, by ANOVA with post hoc Tukey's test.

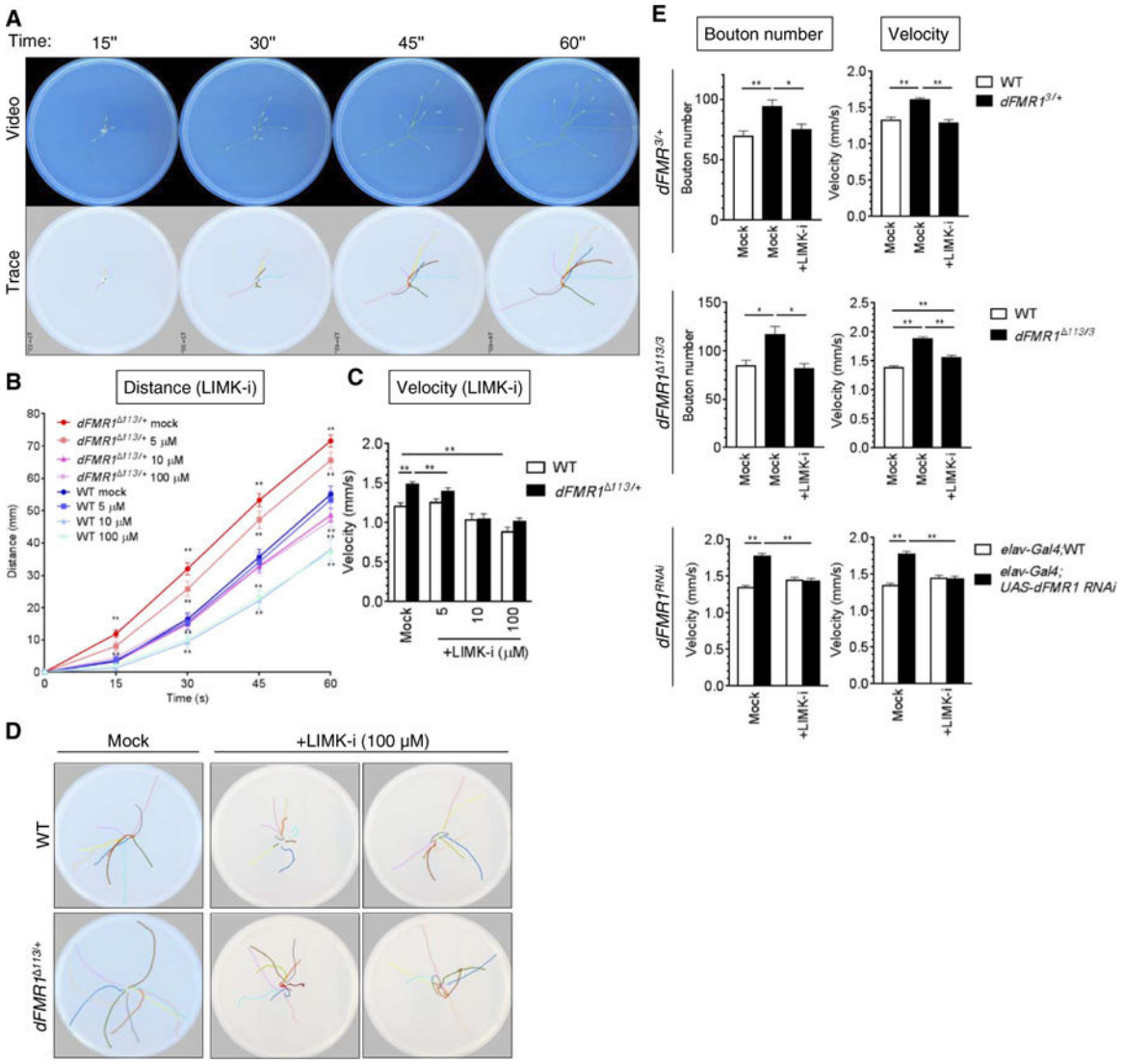

Fig. 3. Development of an algorithm that measures the crawling distance of larvae

(**A**) Representative video images and path analysis data of WT larvae crawling assay. The snapshots of video imaged every 15 s (top) were used to trace a travel path for each individual larva by the LarvaTrack algorithm and shown with lines of different colors (bottom). (**B**) *dFMR1*$^{\Delta 113/+}$ or WT third-instar larvae were treated with LIMK-i (5, 10, or 100 μM) and subjected to the crawling assay. Ten larvae were analyzed simultaneously, and the assay was repeated four times. The average travel distance was quantitated by LarvaTrack. Data are means ± SEM. (**C**) The velocity was calculated on the basis of the plot shown in (B). Data are means ± SEM. $^{**}P < 0.01$, by ANOVA with post hoc Tukey's test. (**D**) Crawling paths of larvae treated with dimethyl sulfoxide (DMSO) (mock) or LIMK-i (100 μM). Each color indicates a crawling path of an individual larva (*dFMR1*$^{\Delta 113/+}$) for 1 min. (**E**) The NMJ bouton number (left) and the velocity (right) were examined in the third-instar larvae of WT, *dFMR1*$^{3/+}$ (top) or *dFMR1*$^{\Delta 113/3}$ (middle) or of *elav-Gal4* or *elav-Gal4;UAS-dFMR1 RNAi* (*dFMR1*^{RNAi}) (bottom), treated with DMSO (mock) or LIMK-i (5 μM top, middle; 10 μM bottom). Data are means ± SEM of at least 18 independent images

of muscle 6/7 in segment A3 (left). The crawling from 10 larvae was analyzed simultaneously, and the assay was repeated five times. The velocity was calculated by the LarvaTrack. Data are means ± SEM. *$P < 0.05$ and **$P < 0.01$, by two-way ANOVA with post hoc Tukey's test.

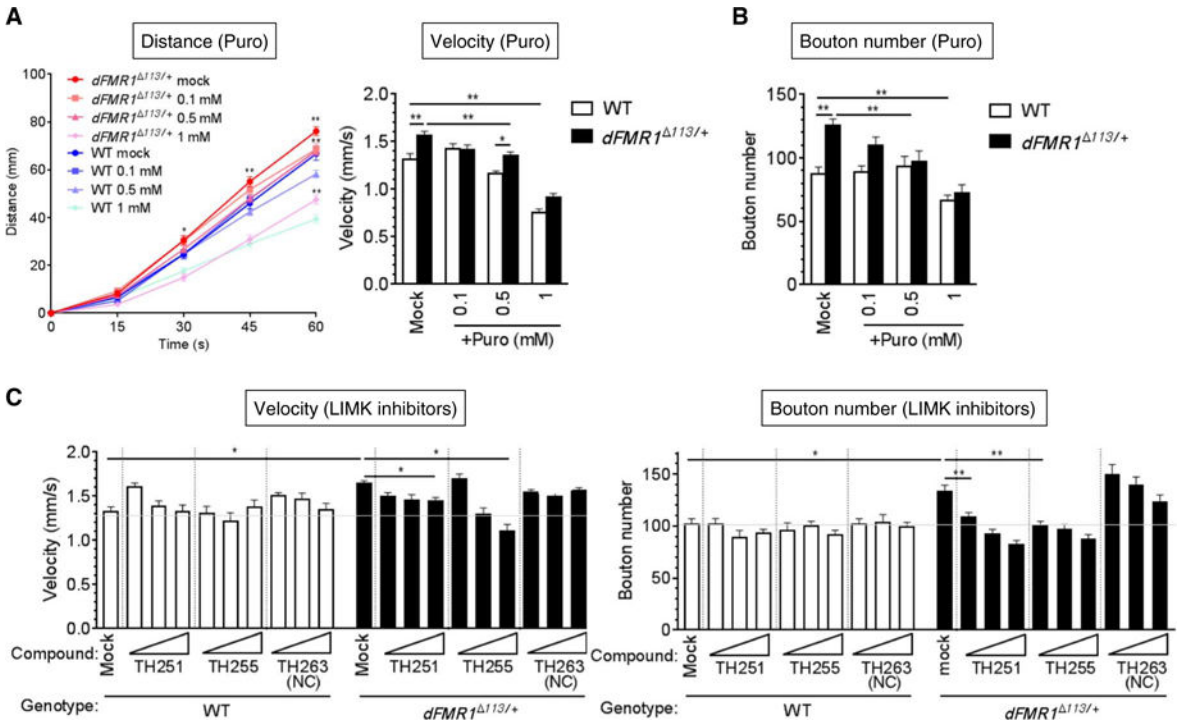

Fig. 4. Administration of a translational inhibitor or a LIMK antagonist rescues the bouton and the crawling phenotype in *dFMR1* mutants

(**A**) *dFMR1*$^{\Delta 113/+}$ or WT third-instar larvae were treated with puromycin (Puro) (0.1, 0.5, or 1 mM) and subjected to the crawling assay. Ten larvae were analyzed simultaneously. The assay was repeated four times. The velocity was calculated, and the average travel distance was quantitated by LarvaTrack. Data are means ± SEM.*$P < 0.05$ and **$P < 0.01$, by ANOVA with post hoc Tukey's test. (**B**) WT or *dFMR1*$^{\Delta 113/+}$ mutant third-instar larvae were treated with increasing doses of puromycin (Puro) as indicated, and bouton numbers were counted. Data are means ± SEM of at least 12 independent images of muscle 6/7 in segment A3. **$P < 0.01$, by ANOVA with post hoc Tukey's test. (**C**) The velocity (left) and the NMJ bouton number (right) were examined in *dFMR1*$^{\Delta 113/+}$ or WT third-instar larvae treated with a LIMK antagonist (TH251 or TH255) (1, 5, or 50 μM) or an inactive analog (TH263). The crawling from 10 larvae was analyzed simultaneously, and the assay was repeated four times. The velocity was calculated by LarvaTrack. Data are means ± SEM. The average number of boutons was calculated from at least 15 independent images of muscle 6/7 in segment A3.*$P < 0.05$ and **$P < 0.01$, by two-way ANOVA with post hoc Dunnett's test. NC, negative control.

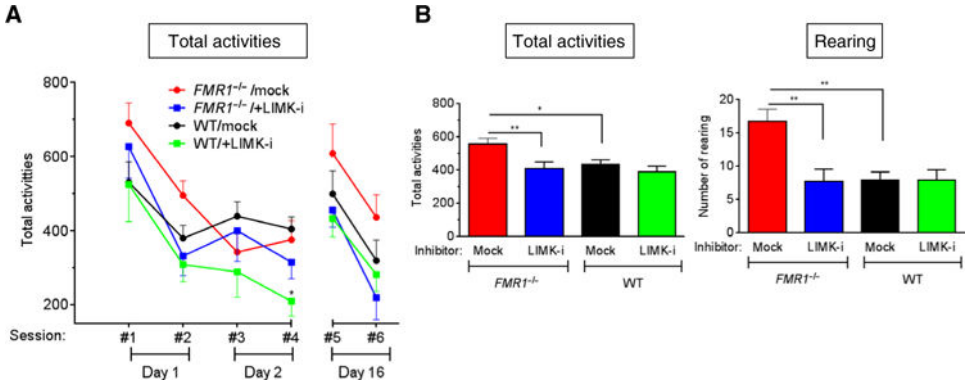

Fig. 5. Administration of LIMK-i ameliorates neuromorphological and behavioral abnormalities in mouse model of FXS

(**A** and **B**) The *FMR1*-KO mice or WT littermates received vehicle (DMSO) alone (mock) or LIMK-i and were subjected to the rOFT at 3 to 3.5 months of age. The number of total activities (A) was counted during six sessions spanning 16 days (#1 and #2 on day 1, #3 and #4 on day 2, and #5 and #6 on day 16). (B) The total activities (left) and rearing behavior (right) during the first two and the last two sessions (sessions #1, #2, #5, and #6) were computed, and the averages per session are indicated. Data are means ± SEM.* $P<0.05$ and ** $P<0.01$, by ANOVA with posthoc Tukey's test. $n=9$ mice for the $FMR1^{-/-}$/mock group. $n = 11$ for $FMR1^{-/-}$/+LIMK-i. $n = 10$ for WT/mock. $n = 7$ for WT/+LIMK-i.